Inorganic Chemistry

Article

pubs.acs.org/IC

Antimony Tartrate Transition-Metal–Oxo Chiral Clusters

Qiang Gao, Xiqu Wang, Joshua Tapp, Angela Moeller, and Allan J. Jacobson*

Department of Chemistry, University of Houston, Houston, Texas 77204-5003, United States

Supporting Information

ABSTRACT: A chiral precursor K_2Sb_2(L-tartrate)$_2$ was used for the assembly of three homochiral heterometallic antimony(III)–tartrate transition-metal–oxo clusters: $Mn(H_2O)_6$-$[Fe_4Mn_4Sb_6(\mu_4\text{-}O)_6(\mu_3\text{-}O)_2$(L-tartrate)$_6(H_2O)_8]\cdot 10.5H_2O$ (**1**), $[V_4Mn_5Sb_6(\mu_4\text{-}O)_6(\mu_3\text{-}O)_2$(L-tartrate)$_6(H_2O)_{13}]\cdot 9.5H_2O$ (**2**), and $(H_3O)[Ni(H_2O)_6]_2[NiCrSb_{12}(\mu_3\text{-}O)_8(\mu_4\text{-}O)_3$(L-tartrate)$_6]\cdot 6H_2O$ (**3**). In **1** and **2**, the antimony tartrate dimer precursor decomposes and recombines to form $Sb_3(\mu_3\text{-}O)$(L-tartrate)$_3$ chiral trimers, which act as scaffolds to construct negative-charged $[Fe_4Mn_4Sb_6(\mu_4\text{-}O)_6(\mu_3\text{-}O)_2$(L-tartrate)$_6]^{2-}$ in **1** and neutral $[V_4Mn_5Sb_6(\mu_4\text{-}O)_6(\mu_3\text{-}O)_2$(L-tartrate)$_6]$ in **2**. The scaffold is flexible and accommodates different types of transition-metal–oxo clusters due to the different possible coordination modes of the L-tartrate ligand. In **3**, a two-level chiral scaffold $Sb_3(\mu_3\text{-}O)$(L-tartrate)$_3Sb_3$ is formed from the precursor. Two such scaffolds are linked by three bridging oxygen atoms to form a cavity occupied by one Cr^{3+} ion and one Ni^{2+} ion disordered over two positions. Cr^{3+} and Ni^{2+} ions are located in two face-shared MO_6 octahedra at the center of a negatively charged $[NiCrSb_{12}(\mu_3\text{-}O)_8(\mu_4\text{-}O)_3$(L-tartrate)$_6]^{3-}$ cluster.

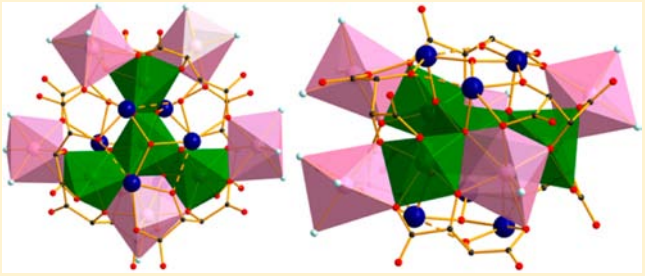

INTRODUCTION

Research on metal clusters in recent decades has been inspired by their structural chemistry as well as by their potential applications in many fields, such as catalysis,[1] photoluminescence,[2] and magnetism.[3] Various types of metal clusters have been discovered and studied, including polyoxometalates, metal–chalcogenide and halide clusters, lanthanide hydroxo compounds, and heterometallic oxo clusters containing both d- and f-block metals.[4] Designed synthesis of clusters with specific nuclearity and charge remains a significant synthetic challenge. Some types of clusters, e.g., polyoxometalates, are constructed using templates, such as phosphates,[5] germanates,[6] silicates,[7] and tellurites,[8] but in other cases no clear synthetic rationale exists. It is of interest to develop a routine way to construct the metal clusters.

Transition-metal–oxo clusters have been of special interest as single molecular magnets (SMM).[9] Multifunctional materials are also of considerable interest because the combination of distinct functionalities may give rise to new interesting phenomena,[10] for example, introduction of chirality into magnetic clusters may cause the magneto-chiral dichroism (MChD) effect.[10c] To date, the most predictable strategy to introduce chirality into targeted materials is using enantiomerically pure ligands as starting materials.[11]

We are interested in using the well-known chiral tartrate dimer $K_2Sb_2L_2$ (H_4L = L-tartaric acid), namely, dipotassium bis(μ-tartrato)diantimony(III) ("tartar emetic") as a starting material for synthesis of new chiral compounds.[12] In this dimer, each L-tartrate bridges two antimony(III) ions in a chelating mode, with two O atoms from two carboxylate groups and another two from the hydroxyl groups. Each Sb^{3+} ion is four coordinated, with the electron lone pairs pointing outward.[12a]

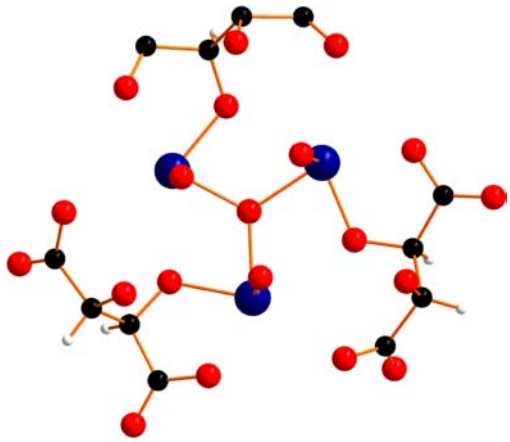

Figure 1. $Sb_3(\mu_3\text{-}O)$ trimer with three dangling L-tartrate ligands. Sb, C, O, and H atoms are represented by blue, black, red, and white circles, respectively.

In our previous work, we demonstrated that this dimer can undergo decomposition and recombination to form a $Sb_3(\mu_3$-O) trimer with three dangling L-tartrate ligands on one side, while the other side of the trimer is terminated by the lone pair Sb(III) cations which act as "structural scissors".[13] This arrangement gives rise to a new type of chiral scaffold (Figure 1). Compounds can then be formed by sandwiching transition-metal–oxo clusters between two such scaffolds.

Following our previous work on antimony–tartrate iron–oxide clusters, we extended the synthesis of homochiral

Received: March 14, 2013
Published: May 15, 2013

   dx.doi.org/10.1021/ic4006345 | Inorg. Chem. 2013, 52, 6610–6616

Table 1. Crystallographic Data for 1−3

	1	2	3
empirical formula	$C_{24}H_{61}Fe_4Mn_5O_{68.5}Sb_6$	$C_{24}H_{54}V_4Mn_5O_{65}Sb_6$	$C_{24}H_{51}CrNi_3O_{66}Sb_{12}$
fw	2674.33	2591.63	3084.78
cryst syst	orthorhombic	monoclinic	hexagonal
space group	$P2_12_12_1$	$P2_1$	$P6_322$
a [Å]	18.6454(8)	10.0553(6)	13.3451(2)
b [Å]	18.645(8)	23.8161(14)	13.3451(2)
c [Å]	20.4827(9)	14.3948(9)	23.8732(6)
α [deg]	90.00	90.00	90.00
β [deg]	90.00	103.025(1)	90.00
γ [deg]	90.00	90.00	120.00
V [Å^3]	7120.8(4)	3358.5(4)	3682.01(12)
Z	4	2	2
D_{calcd} [g/cm^{-3}]	2.495	2.589	2.782
μ [mm^{-1}]	4.006	3.933	5.333
Flack x	−0.005(11)	0.01(2)	0.01(3)
goodness-of-fit on F^2	1.035	0.964	1.097
final R indices [$I > 2\sigma(I)$][a]	R_1 = 0.0246, wR_2= 0.0671	R_1= 0.0463, wR_2 = 0.0717	R_1 = 0.0192, wR_2 = 0.0556
R indices (all data)	R_1 = 0.0275, wR_2 = 0.0685	R_1 = 0.0665, wR_2 = 0.720	R_1 = 0.0201 wR_2 = 0.0559

sandwich clusters to clusters containing other transition metals and obtained three new compounds: $Mn(H_2O)_6[Fe_4Mn_4Sb_6(\mu_4\text{-}O)_6(\mu_3\text{-}O)_2(\text{L-tartrate})_6(H_2O)_8]\cdot 10.5H_2O$ (**1**), $V_4Mn_5Sb_6(\mu_4\text{-}O)_6(\mu_3\text{-}O)_2(\text{L-tartrate})_6(H_2O)_{13}]\cdot 9.5H_2O$ (**2**), and $(H_3O)[Ni(H_2O)_6]_2[NiCrSb_{12}(\mu_3\text{-}O)_8(\mu_4\text{-}O)_3(\text{L-tartrate})_6]\cdot 6H_2O$ (**3**).

In **1** and **2**, the antimony tartrate dimer precursor decomposes and recombines to form $Sb_3(\mu_3\text{-}O)(\text{L-tartrate})_3$ trimers, which act as scaffolds to construct negative-charged $[Fe_4Mn_4Sb_6(\mu_4\text{-}O)_6(\mu_3\text{-}O)_2(\text{L-tartrate})_6]^{2-}$ in **1** and neutral $[V_4Mn_5Sb_6(\mu_4\text{-}O)_6(\mu_3\text{-}O)_2(\text{L-tartrate})_6]$ in **2**. The scaffold is flexible in accommodating different types of transition-metal−oxo clusters due to the versatile coordination modes of the L-tartrate ligand. In **3**, a two-level chiral scaffold $Sb_3(\mu_3\text{-}O)(\text{L-tartrate})_3Sb_3$ is formed from the precursor. Two such scaffolds are linked by three bridging oxygen atoms to form a cavity occupied by one Cr^{3+} ion and one Ni^{2+} ion disordered over two positions. Metal ions are located in two face-shared MO_6 octahedra, forming a negatively charged $[NiCrSb_{12}(\mu_3\text{-}O)_8(\mu_4\text{-}O)_3(\text{L-tartrate})_6]^{3-}$ cluster.

EXPERIMENTAL SECTION

Materials and Methods. All of the reactants were reagent grade and used as purchased. IR spectra were measured on PerkinElmer Spectrum 100 FT-IR spectrometer. Thermogravimetric analysis (TGA) measurements were carried out using a TA Instruments Hi-Res 2950 system in air flow with a heating rate of 5 °C min^{-1}. Elemental analyses were performed by Galbraith Laboratories (Knoxville, TN). Powder X-ray diffraction (PXRD) patterns were collected at room temperature on a Phillps X'pert Pro diffractometer. Magnetic susceptibility measurements were made using a Quantum Design Physical Property Measurement System (QD-PPMS) in the temperature range 2−300 K with an applied field of 500 Oe (zfc, fc). Field-dependent magnetization was recorded at 2 K in fields up to 8 T.

Synthesis of $Mn(H_2O)_6[Fe_4Mn_4Sb_6(\mu_4\text{-}O)_6(\mu_3\text{-}O)_2(\text{L-tartrate})_6(H_2O)_8]\cdot 10.5H_2O$ (1). **1** was synthesized by hydrothermal reaction of a mixture of $Fe(ClO_4)_3$ (71.0 mg, 0.2 mmol), $K_2Sb_2(\text{L-tartrate})_2$ (92.0 mg, 0.15 mmol), $Mn(OAc)_2$ (43.3 mg, 0.25 mmol), and H_2O (6 mL). The mixture was heated at 100 °C in a sealed Teflon vessel for 3 days. Using vacuum filtration and drying in air, orange needle crystals of **1** were recovered as the major phase together with a minor yellow impurity. Yield: 64% based on Fe. Anal. Calcd for $C_{24}H_{61}Fe_4Mn_5O_{68.5}Sb_6$: H, 2.30; C, 10.78; Fe, 8.35; Mn, 10.27; Sb, 27.3. Found: H, 2.07; C, 10.71; Fe, 8.12; Mn, 9.54; Sb, 26.3. IR: 3366(br w), 2968(m), 1624(s), 1346(s), 1114(m), 1055(s), 1033(s), 912(w), 856(w), 812(w), 650(s).

Synthesis of $[V_4Mn_5Sb_6(\mu_4\text{-}O)_6(\mu_3\text{-}O)_2(\text{L-tartrate})_6(H_2O)_{13}]\cdot 9.5H_2O$ (2). **2** was synthesized by hydrothermal reaction of a mixture of VCl_3 (34.0 mg, 0.2 mmol), $Mn(OAc)_2$ (43.3 mg, 0.25 mmol), $K_2Sb_2(\text{L-tartrate})_2$ (62.5 mg, 0.15 mmol), $NaN(CN)_2$ (18.0 mg, 0.2 mmol), H_2O (4 mL), and DMF (2 mL). The mixture was heated at 100 °C in a sealed Teflon vessel for 3 days. Using vacuum filtration and drying in air, green plate crystals of **2** were recovered as major phase together with a few white impurities. Yield: 42% based on V. Anal. Calcd for $C_{24}H_{54}V_4Mn_5O_{65}Sb_6$: H, 2.10; C, 11.12; V, 7.86; Mn, 10.60; Sb, 28.19. Found: H, 1.96; C, 11.04; V, 7.40; Mn, 10.7; Sb, 26.6. IR: 3345(br w), 2922(m), 1618(s), 1346(s), 1132(s), 1056(s), 1032(s), 907(m), 856(m), 730(w), 649(s).

Synthesis of $(H_3O)[Ni(H_2O)_6]_2[NiCrSb_{12}(\mu_3\text{-}O)_8(\mu_4\text{-}O)_3(\text{L-tartrate})_6]\cdot 6H_2O$ (3). **3** was synthesized by hydrothermal reaction of a mixture of $Cr(NO_3)_3$ (80.0 mg, 0.2 mmol), $K_2Sb_2(\text{L-tartrate})_2$ (184.0 mg, 0.3 mmol), $Ni(NO_3)_2\cdot 6H_2O$ (57.3 mg, 0.3 mmol), H_2O (4 mL), and DMF (2 mL). The mixture was heated at 100 °C in a sealed Teflon vessel for 3 days. Using vacuum filtration and drying in air, green block crystals of **3** were recovered as pure phase. Yield: 52% based on Sb. Anal. Calcd for $C_{24}H_{51}CrNi_3O_{66}Sb_{12}$: H, 1.67; C, 9.34; Cr, 1.69; Ni, 5.71; Sb, 47.36. Found: H, 1.70; C, 9.98; Cr, 1.69; Ni, 5.60; Sb, 46.4. IR: 3320(br w), 2980(m), 1625(s), 1356(s), 1129(s), 1066(s), 1033(s), 928(m), 899(m), 847(s), 713(s), 633(s).

Crystallography. Single-crystal X-ray analyses were performed at room temperature on a Siemens SMART platform diffractometer outfitted with an Apex II area detector and monochromatized Mo Kα radiation (λ = 0.71073 Å). Structures were solved by direct methods and refined using the SHELXTL software package.[14] Crystallographic data and structural refinements for compounds **1**−**3** are summarized in Table 1. More details on the crystallographic studies as well as atomic displacement parameters are given in the CIF files. All carbon-bonded hydrogen atoms were placed in geometrically calculated positions; hydrogen atoms in water molecules were not assigned or directly included in the molecular formula.

RESULTS AND DISCUSSION

Description of the Crystal Structures. The coordination modes of L-tartrate ligand are shown in Figures S1−S3, Supporting Information. The following structure discussion is based on the data in the CIF files for **1**−**3**. Formulas of complexes **1**−**3** are further confirmed by elemental analysis (EA) and TG studies.

dx.doi.org/10.1021/ic4006345 | Inorg. Chem. 2013, 52, 6610−6616

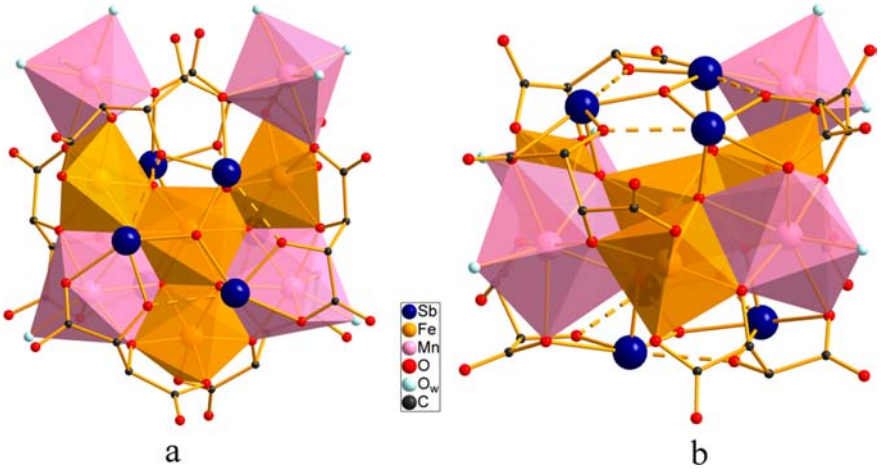

Figure 2. Ball-and-stick representation of $[Fe_4Mn_4Sb_6O_8(L\text{-tartrate})_6]^{2-}$ cluster in **1**: (a) top and (b) side view. Fe^{3+} and Mn^{2+} cations are highlighted as yellow and rose polyhedra, respectively. Dashed lines indicate weak Sb−O bonding.

Compound **1** contains the $[Fe_4Mn_4Sb_6(\mu_4\text{-}O)_6(\mu_3\text{-}O)_2(L\text{-tartrate})_6]^{2-}$ cluster ion. In this cluster ion, two $Sb_3(\mu_3\text{-}O)(L\text{-tartrate})_3$ scaffolds (Figure 1) sandwich a flat $Fe(III)_4Mn(II)_4$ oxo cluster to form the cluster ion (Figure 2). Four Fe(III) cations are arranged in a triangle with one cation at the center and the other three at the vertices, a similar arrangement to that found in the previously reported $Fe(III)_4$ cluster.[13b] Four Mn(II) cations are added to the middle layer through bonding with oxygen atoms from the L-tartrate ligands of the two scaffolds. Two Mn(II) polyhedra are inserted between peripheral Fe(III) octahedra, sharing edges with three adjacent Fe(III) octahedra and almost lying in the $Fe(III)_4$ plane (Figure 2a). They are seven coordinated with four oxygen atoms from two L-tartrate ligands from two scaffolds, two μ_4-O atoms, and one water molecule. The other two Mn(II) ions are six coordinated with two oxygen atoms from two carboxylate groups of two L-tartrate ligands from one scaffold and one oxygen atom from a hydroxyl group of one L-tartrate ligand from the other scaffold. Three water molecules complete the slightly distorted octahedron motif. The octahedra each share one edge with one Fe(III) polyhedron. The distances between the central Fe(III) ion and the two inserted Mn(II) ions are 3.4366(0) and 3.4951(0) Å, and the distances between the central Fe(III) ion and the two dangling Mn(II) ions are 5.5314(2) and 5.5461(2) Å, respectively. The distances between the central and the peripheral Fe(III) ions range from 3.0810(1) to 3.1144(1) Å, comparable to those found in the $Fe(III)_7$ cluster and a little shorter than those in the $Fe(III)_4$ cluster.[13b]

In the $Sb_3(\mu_3\text{-}O)$ unit, the Sb(III) cations and the μ_3-O are arranged in a similar way to the $Fe(III)_4$ cluster, with the μ_3-O atom at the center of a triangle of Sb^{3+} cations. All Sb(III) cations display the typical one-sided coordination environment expected for lone-pair cations. Each Sb(III) cation is coordinated by five oxygen atoms in a distorted tetragonal pyramidal arrangement. There are three types of coordination modes for the six L-tartrate ligands (Figure S1, Supporting Information). In mode A (Figure S1a, Supporting Information), each ligand uses four oxygen atoms from the four functional groups to chelate one Sb(III) and one Fe(III) cation. The hydroxyl oxygen atom coordinating to the Sb(III) cation is also weakly bonded to a second Sb(III) atom, while the other hydroxyl oxygen atom which coordinates to the Fe(III) ion is further connected to one Mn(II) ion. The carboxylate oxygen atom engaged in chelating Sb(III) cation further connects to one Mn(II) ion. Coordination modes B and C are slightly different from mode A in the way the ligand connects to Mn(II) ions. In mode B, two Mn(II) ions are connected to the ligand: the first one is by the carboxylate oxygen chelating the Fe(III) ion; the second ion is chelated by the hydroxyl oxygen atom, which also chelates the Fe(III) ion and the carboxylate oxygen atom chelating the Sb(III) ion. In mode C, only one Mn(II) ion is connected to the ligand, in a similar way as the second one is connected in mode B. Two $Sb(III)_3O$ units are connected to the $Fe(III)_4Mn(II)_4$ cluster from both above and below, each by three L-tartrate ligands in the three coordination modes, leading to a chiral heterometallic sandwich with a thickness of 6.5707(3) Å (distance between the two μ_3-O atoms on the opposite sides, Figure 2).

Each cluster is hydrogen bonded to six adjacent clusters with a O−O distance of 2.646−2.867 Å, generating a three-dimensional supramolecular network with rectangular channels along the *a* axis. The channels have a size of 8.302 × 8.206 Å (diagonal distances). The hydrated Mn(II) ions and guest water molecules are located in the channels (Figure S4, Supporting Information).

Compared with the previously reported Fe_4Mn_3 clusters,[13a] this cluster has one more Mn(II) ion inserted in the outer sphere. Insertion is accomplished by opening of one of the triangular edges formed by the three outer Fe(III) ions, which leaves more space for insertion of the fourth Mn(II) ion. Opening of the cluster is accompanied by a change of the coordination mode of the ligand. In the Fe_4Mn_3 cluster, all ligands adopt mode C (not taking into account the carboxylate oxygen atom connecting to the adjacent clusters) and all Mn(II) ions are chelated by the ligands, while in the Fe_4Mn_4 clusters, there are two more types of coordination modes (A and B). The two Mn(II) ions on the opening edge are connected to the ligands in mode A and mode B in a monodentate fashion. This result demonstrates that the scaffolds are flexible and can accommodate metal−oxo clusters of different sizes in the central region. The flexibility is made possible by the different coordination modes of the L-tartrate ligand.

A neutral cluster $[V_4Mn_5Sb_6(\mu_4\text{-}O)_6(\mu_3\text{-}O)_2(L\text{-tartrate})_6]$ is present in compound **2**. In this cluster, four V(III) ions are

dx.doi.org/10.1021/ic4006345 | *Inorg. Chem.* 2013, 52, 6610−6616

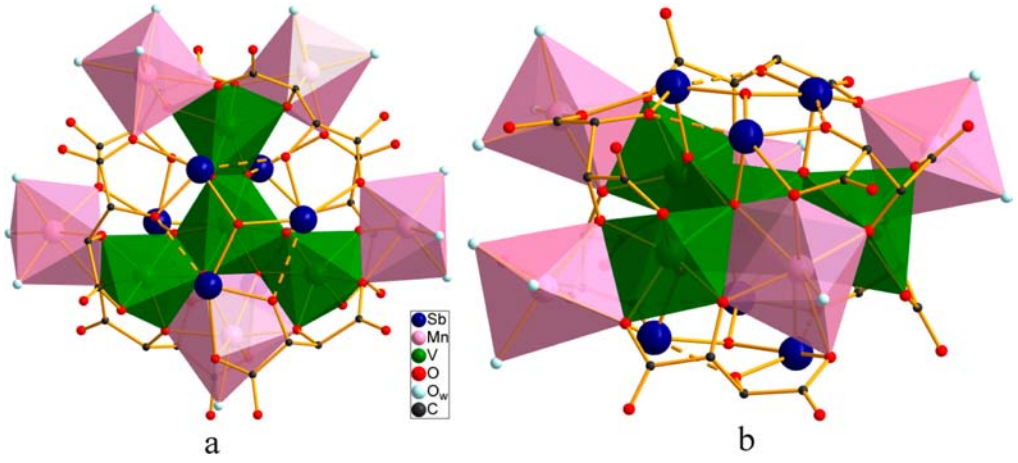

Figure 3. Ball-and-stick representation of $[V_4Mn_5Sb_6O_8(\text{L-tartrate})_6]$ cluster in **2**: (a) top and (b) side view. V^{3+} and Mn^{2+} cations are highlighted as green and rose octahedra. Dashed lines indicate weak Sb−O bonding.

arranged in the same way as the four Fe(III) ions in **1**; the distances between the central V(III) ion and the peripheral V(III) ions are 3.0180(2), 3.0559(2), and 3.0602(1) Å (Figure 3a). All Mn(II) ions are added to the cluster such that Mn(II) polyhedra share edges with the V(III) octahedra. One Mn(II) ion is inserted between two V(III) octahedra on two vertices; it is seven coordinated by four oxygen atoms from two L-tartrate ligands from two scaffolds, two μ_4-O atoms, and one water molecule and lies in the $V(III)_4$ plane. The other four Mn(II) ions are all six coordinated by three oxygen atoms from three L-tartrate ligands and three water molecules. Two of them are connected to the two V(III) octahedra which are connected to the seven-coordinated Mn(II) polyhedron; one lies above and one below the $V(III)_4$ plane. The other two Mn(II) polyhedra are attached to the third peripheral V(III) octahedron on either side of the $V(III)_4$ plane. The distances between the central V(III) ion and five Mn(II) ions are 3.4370 (2), 5.4744 (2), 5.4950 (2), 5.5082 (3), and 5.5165 (3) Å.

The L-tartrate ligand has three types of coordination modes (Figure S2, Supporting Information). Modes A and B (Figure S2a and S2b, Supporting Information) are similar to modes A and B in the Fe_4Mn_4 cluster of **1**, except that the Fe(III) ions are replaced by V(III) ions. In mode C, the ligand coordinates to three Mn(II) ions with two carboxylate oxygen atoms and one hydroxyl atom (Figure S2c, Supporting Information). Two $Sb(III)_3O$ units are connected to the $V(III)_4Mn(II)_5$ cluster from both above and below, each by three L-tartrate ligands in the three coordination modes, forming a chiral heterometallic sandwich with a thickness of 6.6886(3) Å (distance between the two μ_3-O atoms on the opposite sides, Figure 3). Each cluster is hydrogen bonded to 14 adjacent clusters with O−O distances of 2.611−2.924 Å, with guest water molecules residing between the clusters (Figure S5, Supporting Information).

Compared with the Fe_4Mn_4 cluster in **1**, Fe(III) ions are replaced by V(III) ions in the V_4Mn_5 cluster in **2** and one more Mn(II) ion is inserted into the middle metal−oxo layer. This insertion is managed in a similar way to insertion of the fourth Mn(II) ion into the Fe_4Mn_3 cluster. The second triangular edge opens up and the original Mn(II) ion moves outward to afford space for insertion of the fifth Mn(II) ion, which also involves a change in the coordination modes of the L-tartrate ligands. The ligands connecting the Mn(II) ion from the closed edge and the open edge adopt mode B (Figure S2, Supporting Information). Those connecting the Mn(II) ions from the same open edge adopt mode A, while those connecting the Mn(II) ions from two different open edges adopt mode C. This further demonstrates that the type of metal−oxo cluster is closely coupled to the coordination modes of the L-tartrate ligand.

Compound **3** contains a $[NiCrSb_{12}(\mu_3\text{-O})_8(\mu_4\text{-O})_3(\text{L-tartrate})_6]^{3-}$ cluster comprised of two two-level $Sb_3(\mu_3\text{-O})(\text{L-tartrate})_3Sb_3$ scaffolds that are linked by three bridging oxygen atoms to form a cavity (Figure 4).

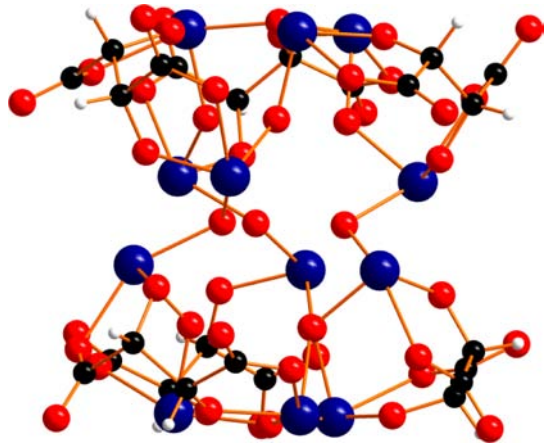

Figure 4. Cavity formed by linking two two-level $Sb_3(\mu_3\text{-O})(\text{L-tartrate})_3Sb_3$ scaffolds. Sb, C, O, and H atoms are represented by blue, black, red, and white circles, respectively.

In this scaffold, the L-tartrate ligand chelates two Sb(III) ions with its carboxylate and hydroxyl groups. It also connects to another two Sb(III) ions with two carboxylate oxygen atoms through weak Sb−O bonding (2.842 and 2.897 Å) (Figure S3, Supporting Information). Three L-tartrate ligands connect the trimer Sb_3O to three Sb(III) ions to form the two-level scaffold. The three additional Sb(III) ions also display the typical one-sided coordination environment expected for lone-pair cations with four strong Sb−O bonds (1.976−2.213 Å) and one weak Sb−O bond (2.897 Å). Compared with the $Sb_3(\mu_3\text{-O})(\text{L-tartrate})_3$ scaffold, these Sb(III) ions are not connected by a μ_3-O atom. Instead, these Sb(III) ions construct a cavity by sharing three oxygen atoms with an adjacent scaffold. The

dx.doi.org/10.1021/ic4006345 | Inorg. Chem. 2013, 52, 6610−6616

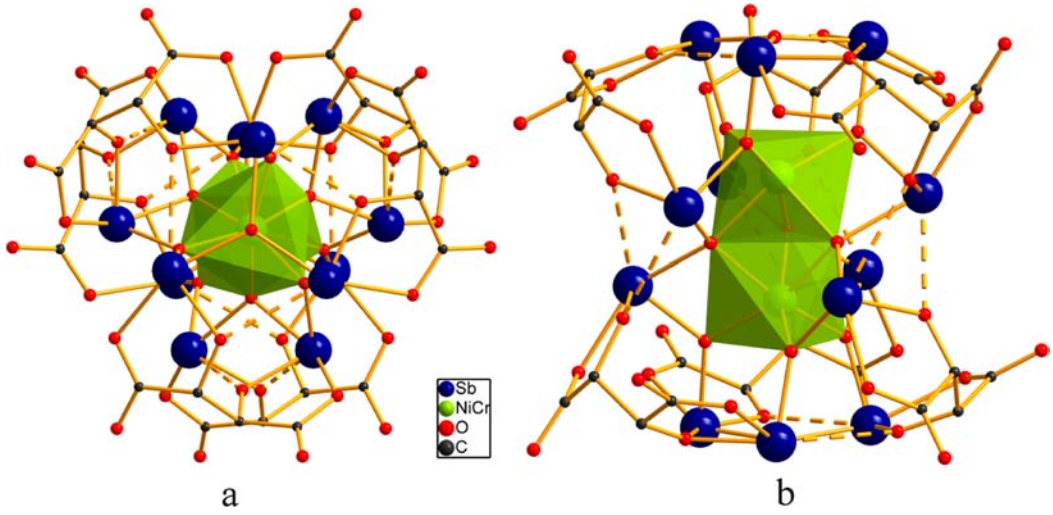

Figure 5. Ball-and-stick representation of $[NiCrSb_{12}O_{11}(L\text{-tartrate})_6]^{3-}$ cluster in **3**: (a) top and (b) side view. Disordered Cr^{3+}/Ni^{2+} are highlighted as lime octahedra. Dashed lines indicate weak Sb−O bonding.

cavity is occupied by one Cr^{3+} ion and one Ni^{2+} ion in octahedral coordination. The octahedra share a face, and metal ions are disordered over the two positions (Figure 5). The result is a four-level heterometallic homochiral cluster $[NiCrSb_{12}(\mu_3\text{-O})_8(\mu_4\text{-O})_3(L\text{-tartrate})_6]^{3-}$. The negatively charged cluster is charge balanced by a hydrated $Ni(H_2O)_6^{2+}$ ion and a protonated water molecule. Each $Ni(H_2O)_6^{2+}$ is connected to six adjacent $[NiCrSb_{12}(\mu_3\text{-O})_8(\mu_4\text{-O})_3(L\text{-tartrate})_6]^{3-}$ clusters through hydrogen bonding (O−O distances = 2.714 and 2.830 Å), which are arranged in a triangle. Protonated and free water molecules are located within and between these triangles (Figure S6, Supporting Information).

We proposed a mechanism for formation of this class of metal−oxo clusters. For the three-layer clusters (Fe_4Na_3,[13b] Fe_7,[13b] Fe_6Na,[13b] Fe_4Mn_3,[13a] Fe_4Mn_4, V_4Mn_5), the central ion (Fe(III) or V(III)) adopts nearly regular octahedral coordination with six μ_3-O or μ_4-O atoms which are bonded to six Sb(III) ions belonging to two scaffolds one above and one below. Peripheral ions can be categorized in three groups depending on their distances from the central ion. In the first group, all three ions (Fe(III) in **1** or V(III) in **2**) have distorted octahedral coordination. This arrangement gives rise to the prototypic structure with four metal ions in a plane. The cluster ion has 10 negative charges which are balanced by Na^+, K^+, or $[(CH_3)_2NH_2]^+$ ions. In these prototypic structures, three spaces are present between three peripheral transition-metal ions. The spaces contain four O atoms from two L-tartrate ligands on the outside and two O atoms inside (see Figure 6a). One water molecule completes the coordination environment, resulting in a slightly distorted pentagonal bipyramid.

The two O atoms from two hydroxyl groups of the tartrate ligand bond most strongly with the ion (2.107(3) and 2.078(3) Å) and define the apical positions of the pentagonal bipyramid. Examples are now known with monovalent and divalent metal ions (Na(I), Mn(II), or Fe(II)) in the second group (Table 2). The ions in the first group provide other types of spaces that can accommodate additional metal ions, which differ in their distances from the central ions. In the third group, divalent metal ions (e.g., Mn(II)) only share one edge with one metal ion in the first group. The octahedron is completed by three coordinated water molecules and one carboxylate oxygen atom from a tartrate ligand (Figure 6b). The second group can

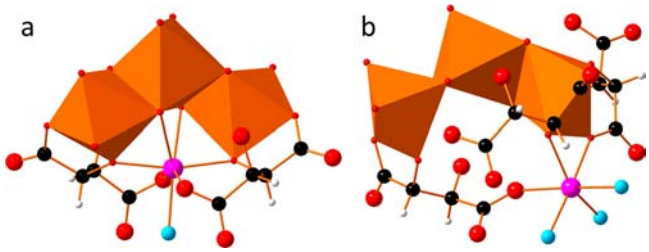

Figure 6. Coordination environments defined by the central group of four octahedra: (a) second group and (b) third group. Group 1 ions are represented as orange octahedra. O, C, and H atoms and the coordinated water molecules are represented as red, black, white, and blue circles, respectively.

Table 2. Examples of Antimony Tartrate Transition-Metal Clusters Containing Metal Ions in Different Distributions

cluster ion	group 1	group 2	group 3
$[Na_3Fe_4Sb_6(\mu_4\text{-O})_6(\mu_3\text{-O})_2(L\text{-tartrate})_6]$	4Fe	3Na	
$[Fe_7Sb_6(\mu_4\text{-O})_6(\mu_3\text{-O})_2(L\text{-tartrate})_6]$	4Fe	3Fe	
$[Fe_4Mn_3Sb_6(\mu_4\text{-O})_6(\mu_3\text{-O})_2(L\text{-tartrate})_6(H_2O)]$	4Fe	3Mn	
$[Fe_4Mn4Sb6(\mu_4\text{-O})_6(\mu_3\text{-O})_2(L\text{-tartrate})_6(H_2O)_8]$	4Fe	2Mn	2Mn
$[V_4Mn_5Sb_6(\mu_4\text{-O})_6(\mu_3\text{-O})_2(L\text{-tartrate})_6(H_2O)_{13}]$	4V	1Mn	4Mn

accommodate up to three seven-coordinated metal ions, while the third group can hold theoretically up to six-coordinated metal ions. Assembly is mainly controlled by the ion radius and coordination modes of the ions and ligands. For the four-layer cluster, the precursor $Sb_2(L\text{-tartrate})_2^{2-}$ decomposes in a slightly different way: only one L-tartrate ligand dissociates from the precursor, and the remaining part recombines into the two level scaffold. Two such scaffolds are connected by three bridging oxygen atoms to form a cavity. The cavity is occupied by one Cr^{3+} ion and one Ni^{2+} ion in octahedral coordination. The octahedra share a face, and the metal ions are disordered over the two positions.

The middle layers of the Fe_4Mn_4 clusters in **1** and V_4Mn_5 clusters in **2** may be considered as intermediates between fragments of the brucite-type layer and the gibbsite-type layer.

dx.doi.org/10.1021/ic4006345 | Inorg. Chem. 2013, 52, 6610−6616

The middle layer of the Fe_7 cluster may be considered as a hexagon fragment of a brucite-type layer. As the larger Mn^{2+} ions replace the Fe^{2+} ions, the layer changes toward the less dense gibbsite type. The V_4 core in **2** is slightly more compact than the Fe_4 core in **1**, and the V_4Mn_5 layer is closer to the gibbsite type. A gibbsite-type M_4Mn_6 middle layer is expected for a M_4 core of even smaller metal ions.

THERMOGRAVIMETRIC ANALYSIS

The phase purity of the compounds was confirmed by comparison of the measured powder X-ray diffraction patterns with patterns simulated from the single-crystal data (Figures S7–S9, Supporting Information). Thermal stabilities were investigated, and the results are shown in Figures S10–S12, Supporting Information. **1** gradually loses lattice water molecules and coordinated water molecules from the cluster up to 265 °C (18.5 water molecules, calcd 12.45%, found 13.19%), and then it decomposes abruptly to give a residue of a mixture of Fe_2O_3, Mn_3O_4, and Sb_2O_5 (calcd 64.49%, found 64.59%). **2** loses lattice water molecules and part of the coordinated water molecules (13 water molecules, calcd 9.0%, found 9.1%) and reach a plateau from 112 to 163 °C; then it loses weight gradually in a series of steps to give a residue of a mixture of Mn_3O_4, VO_2, and Sb_2O_5 (calcd 64.3%, found 65.0%). **3** loses its free water molecules as well as coordinated water molecules up to 255 °C (19 water molecules, calcd 11.09%, found 10.7%); then the ligands decompose to give a mixture of NiO, Sb_2O_3, and Cr_2O_3 at 440 °C (calcd 66.4%, found 66.9%) and then stabilizes up to 480 °C.

MAGNETIC MEASUREMENTS

Magnetic susceptibility data multiplied by temperature ($\chi_M T$) as measured in fields of 500 Oe are shown in Figure 7. It should

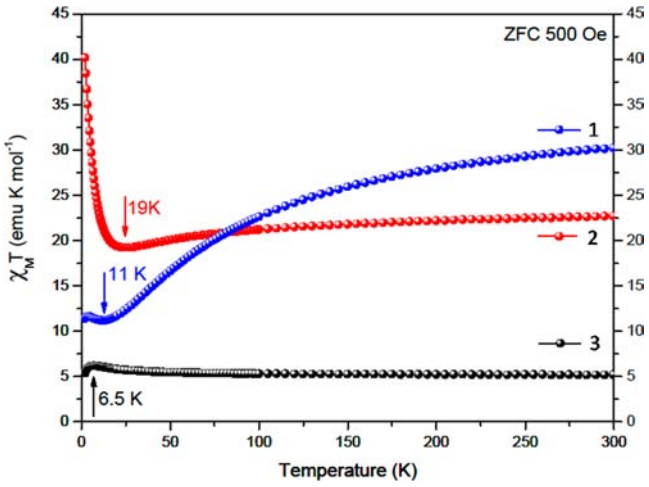

Figure 7. $\chi_M T$ versus temperature for compounds **1**–**3**.

be noted that zero-field and field-cooled measurements were identical. We evaluated data using the effective Curie constant, $C = \chi T$, in order to estimate the effective spin in relation to the structural arrangements within each cluster for **1**–**3**. More details are given in the Supporting Information.

For **1** the high-temperature limit is found to be χT = 30.2 emuK/mol, as expected for all Mn^{2+} ions essentially uncoupled, but the $[Fe^{3+}{}_4]$-core is ordered with the central Fe ion antiparallel to the three surrounding Fe^{3+} (theor 35.0 emuK/mol). On lowering the temperature, the surrounding 5 Mn^{2+} ions forming the outer ring start to align antiferromagnetically indicated by the minimum around 11 K (exp. 11.3 emu K/mol, theor 13.1 emu K/mol). A small discrepancy is observed, however, which might be attributed to one Mn^{2+} ion in the structure that is not part of the cluster ion, adding some antiferromagnetic interaction, thus slightly lowering the overall χT value. Compound **2** consists of a $[V^{3+}{}_4]$ core with 5 Mn^{2+} forming the outer ring and no isolated ions. This situation is similar to the previous one. At high temperatures the core spins are aligned antiferromagnetically and the ions of the ring remain uncoupled (exp. 22.7 emu K/mol, theor 23.9 emu K/mol). Approaching lower temperatures, a minimum is observed at 19 K corresponding to the antiparallel alignment of the ring members (exp. 19.3 emu K/mol, theor. 19.9 emu K/mol). Overall, since the spin systems are different V^{3+}, d^2, and Mn^{2+}, d^5, the remaining moment equivalent to an effective spin of 10.5 remains and produces the upturn at very low temperatures, see also M(H) (Figure S17, Supporting Information). **3** consists of two isolated Ni^{2+} ions and a core formed by face-sharing Ni^{2+}, d^8, and Cr^{3+}, d^3. For the latter an effective ferromagnetic interaction is derived from the almost constant temperature dependence of χT of 5.2 emu K/mol (theor 4.9) only slightly increasing around 6.5 K. Confirmation of this ground state is further obtained from M(H) data (Figure S17, Supporting Information).

CONCLUSION

In summary, three homochiral heterometallic clusters composed of antimony tartrate transition-metal–oxo sandwiches have been obtained using a water-soluble chiral dimer Sb_2(L-tartrate)$_2{}^{2-}$ as the precusor. These clusters consist of two different types of scaffolds. A comparison of **1** and **2** with the previously reported Fe_4Na_3, Fe_7, Fe_6Na, and Fe_4Mn_3 clusters shows that the number and types of cations in the middle layer of the sandwich can be varied, indicating the flexibility of the chiral scaffold, which is attributed to the versatile coordination modes of the L-tartrate ligand. The two-level scaffold in **3** demonstrates that other different types of chiral scaffolds may be derived from the same precusor.

ASSOCIATED CONTENT

Supporting Information

X-ray crystallographic information files (CIF) for compounds **1**–**3**, additional structure figures, and physical characterization data for **1**–**3**. This material is available free of charge via the Internet at http://pubs.acs.org.

AUTHOR INFORMATION

Corresponding Author

*Phone: 713-743-2785. Fax: 713-743-2787. E-mail: ajjacob@uh.edu.

Notes

The authors declare no competing financial interest.

ACKNOWLEDGMENTS

We thank the R. A. Welch Foundation (nos. E-0024 and G-099857) for support of this work.

REFERENCES

(1) (a) Dietl, N.; Höckendorf, R. F.; Schlangen, M.; Lerch, M.; Beyer, M. K.; Schwarz, H. *Angew. Chem., Int. Ed.* **2011**, *50*, 1430. (b) Kamata,

K.; Yamaura, T.; Mizuno, N. *Angew. Chem., Int. Ed.* **2012**, *51*, 7275. (c) Tanaka, S.; Annakaab, M.; Sakai, K. *Chem. Commun.* **2012**, 1653. (d) Kopilevich, S.; Gil, A.; Garcia-Ratés, M.; Bonet-Ávalos, J.; Bo, C.; Müller, A.; Weinstock, I. A. *J. Am. Chem. Soc.* **2012**, *134*, 13082.

(2) (a) Yue, C. Y.; Yan, C. F.; Feng, R.; Wu, M. Y.; Chen, L.; Jiang, F. L.; Hong, M. C. *Inorg. Chem.* **2009**, *48*, 2873. (b) Sun, D.; Wang, D. F.; Han, X. G.; Zhang, N.; Huang, R. B.; Zheng, L. S. *Chem. Commun.* **2011**, 746.

(3) (a) Zhang, L.; Clérac, R.; Heijboer, P.; Schmitt, W. *Angew. Chem., Int. Ed.* **2012**, *51*, 3007. (b) Schray, D.; Abbas, G.; Lan, Y. H.; Mereacre, V.; Sundt, A.; Dreiser, J.; Waldmann, O.; Kostakis, G. E.; Anson, C. E.; Powell, A. K. *Angew. Chem., Int. Ed.* **2010**, *49*, 5185. (c) Kong, X. J.; Ren, Y. P.; Long, L. S.; Zheng, Z. P.; Huang, R. B.; Zheng, L. S. *J. Am. Chem. Soc.* **2007**, *129*, 7016. (d) Gui, L. C.; Wang, X. J.; Ni, Q. L.; Wang, M.; Liang, F. P.; Zou, H. H. *J. Am. Chem. Soc.* **2012**, *134*, 852. (e) Bogani, L.; Wernsdorfer, W. *Nat. Mater.* **2008**, *7*, 179. (f) Anwar, M. U.; Louise N. Dawe, L. N.; Alam, M. S.; Thompson, L. K. *Inorg. Chem.* **2012**, *51*, 11241.

(4) (a) Sokolow, J. D.; Trzop, E.; Chen, Y.; Tang, J. J.; Allen, L. J.; Crabtree, R. H.; Benedict, J. B.; Coppens, P. *J. Am. Chem. Soc.* **2012**, *134*, 11695. (b) Zeng, Y. F.; Hu, X.; Xue, L.; Liu, S. J.; Hu, T. L.; Bu, X. H. *Inorg. Chem.* **2012**, *51*, 9571. (c) Zhuang, G. L.; Chen, W. X.; Hai-Xia Zhao, H. X.; Kong, X. J.; Long, L. S.; Huang, R. B.; Zheng, L. S. *Inorg. Chem.* **2011**, *50*, 3843. (d) Hu, B.; Feng, M. L.; Li, J. R.; Lin, Q. P.; Huang, X. Y. *Angew. Chem., Int. Ed.* **20011**, *50*, 8110. (e) Ling, J.; Qiu, J.; Burns, P. C. *Inorg. Chem.* **2012**, *51*, 2403.

(5) (a) Nohra, B.; Moll, H. E.; Albelo, L. M. R.; Mialane, P.; Marrot, J.; Mellot-Draznieks, C.; O'Keeffe, M.; Biboum, R. N.; Lemaire, J.; Keita, B.; Nadjo, L.; Dolbecq, A. *J. Am. Chem. Soc.* **2011**, *133*, 13363. (b) Li, X. X.; Zheng, S. T.; Zhang, J.; Fang, W. H.; Yang, G. Y.; Clemente-Juan, J. M. *Chem.—Eur. J.* **2011**, 13032. (c) Miras, H. N.; Sorus, M.; Hawkett, J.; Sells, D. O.; McInnes, E. J. L.; Cronin, L. *J. Am. Chem. Soc.* **2012**, *134*, 6980. (d) Pang, H. J.; Peng, J.; Zhang, C. J.; Li, Y. G.; Zhang, P. P.; Ma, H. Y.; Su, Z. M. *Chem. Commun.* **2010**, 5097.

(6) Reinoso, S.; Giménez-Marqués, M.; Galán-Mascarós, J. R.; Vitoria, P.; Gutiórrez-Zorrilla, J. M. *Angew. Chem., Int. Ed.* **2010**, *49*, 8384.

(7) (a) Bassil, B. S.; Kortz, U.; Tigan, A. S.; Juan M. Clemente-Juan, J. M.; Keita, B.; Oliveira, P.; Nadjo, L. *Inorg. Chem.* **2005**, *44*, 9360. (b) Wang, X. L.; Hu, H. L.; Tian, A. X.; Lin, H. Y.; Li, J. *Inorg. Chem.* **2010**, *49*, 10299.

(8) (a) Corella-Ochoa, M. N.; Miras, H. N.; Kidd, A.; Long, D. L.; Cronin, L. *Chem. Commun.* **2011**, 8799. (b) Huang, X. H.; Huang, C. C.; Liu, D. S.; Liu, Z. Q.; Wang, Y. B. *Cryst. Growth Des.* **2010**, *10*, 2021.

(9) (a) Chen, S. Y.; Beedle, C. C.; Pei-Rung Gan, P. R.; Gene-Hsian Lee, G. H.; Stephen Hill, S.; Yang, E. C. *Inorg. Chem.* **2012**, *51*, 4448. (b) Fang, X. K.; Kögerler, P.; Speldrich, M.; Schilderb, H.; Luban, M. *Chem. Commun.* **2011**, 1218. (c) Nguyen, T. N.; Wernsdorfer, W.; Abboud, K. A.; Christou, G. *J. Am. Chem. Soc.* **2011**, *133*, 20688.

(10) (a) Seo, J. S.; Whang, D.; Lee, H.; Jun, S. I.; Oh, J.; Jeon, Y. J.; Kim, K. *Nature* **2000**, *404*, 982. (b) Rabone, J.; Yue, Y. F.; Chong, S. Y.; Stylianou, K. C.; Bacsa, J.; Bradshaw, D.; Darling, G. R.; Berry, N. G.; Khimyak, Y. Z.; Ganin, A. Y.; Wiper, P.; Claridge, J. B.; Rosseinsky, M. J. *Science* **2010**, *329*, 1053. (c) Train, C.; Gheorghe, R.; Krstic, V.; Chamoreau, L. M.; Ovanesyan, N. S.; Rikken, G. L. J. A.; Gruselle, M.; Verdaguer, M. *Nat. Mater.* **2008**, *7*, 729.

(11) (a) Joarder, B.; Chaudhari, A. K.; Ghosh, S. K. *Inorg. Chem.* **2012**, *51*, 4644. (b) Ma, L. Q.; Lin, W. B. *Angew. Chem., Int. Ed.* **2009**, *48*, 3637. (c) Xi, X. B.; Fang, Y.; Dong, T. W.; Cui, Y. *Angew. Chem., Int. Ed.* **2011**, *50*, 1154. (d) Gedrich, K.; Senkovska, I.; Baburin, I. A.; Mueller, U.; Trapp, O.; Kaskel, S. *Inorg. Chem.* **2010**, *49*, 4440.

(12) (a) Gao, Q.; Wang, X. Q.; Jacobson, A. J. *Inorg. Chem.* **2011**, *50*, 9073. (b) Gress, M. E.; Jacobson, R. A. *Inorg. Chim. Acta* **1974**, *8*, 209. (c) Sagatys, G.; Smith, D. S.; Lynch, D. E.; Kennard, C. H. L. *J. Chem. Soc. Dalton, Trans.* **1991**, 361. (d) Bohatý, L.; Fröhlich, R.; Tebbe, K.-F. *Acta Crystallogr.* **1983**, *C39*, 59. (e) Palenik, R. C.; Abboud, K. A.; Palenik, G. J. *Inorg. Chim. Acta* **2005**, *358*, 1034.

(13) (a) Gao, Q.; Wang, X. Q.; Jacobson, A. J. *Chem. Commun.* **2012**, 3990. (b) Gao, Q.; Wang, X. Q.; Conato, M. T.; Makarenko, T.; Jacobson, A. J. *Cryst. Growth Des.* **2011**, *11*, 4632.

(14) Sheldrick, G. M. *SHELXTL, Program for Refinement of Crystal Structures*; Siemens Analytical X-ray Instruments: Madison, WI, 1994.